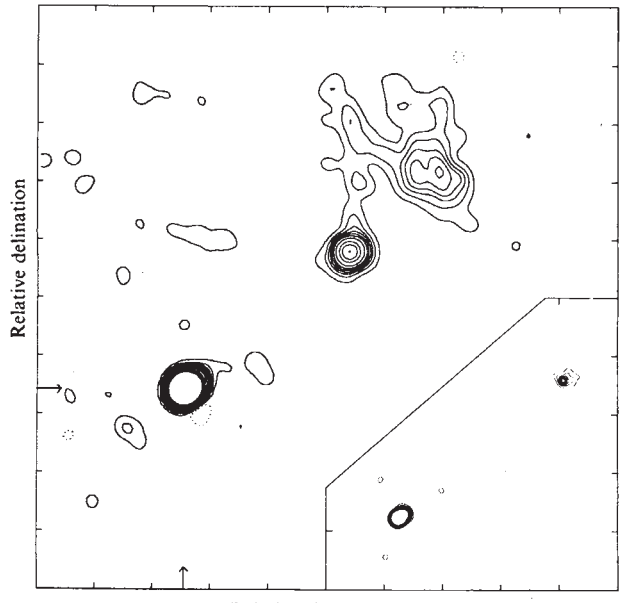

Fig. 3 MERLIN map at 5 GHz showing the structure of the north-west knot complex with a resolution of 0.06 arc s; contour levels 0.2, 0.5, 0.8, 1.1, 1.4, 1.7, 2, 3, 4,... 10% of the peak brightness of 2.11 Jy per beam. The scale corresponds to 0.2 arc s per tick. Inset: EVN map at 1,660 MHz, showing the nucleus and the brightest knot only with a resolution of 0.025 arc s; contour levels 1, 2, 3, 4, 5,... 10% of the peak brightness of 2.28 Jy per beam.

high (up to $\sim$1,000 km s^{-1}). 0351+026 bears a 'striking resemblance'[25] to the quasar 3C48 and this is an important pointer because, like 3C380, 3C48 is a very powerful SSCS with an odd radio structure[21,26]. The galactic-sized nebulosity associated with 3C48 also contains emission-line gas[25,27] moving at high velocity ($\sim$500 km s^{-1}) with respect to the underlying galaxy, which has the spectral characteristics of a spiral[27], that is, a gas-rich object.

Extended gas with the right properties to disturb the beams more strongly than in active galaxies has therefore been directly observed in QSOs. In this context it is worth noting the apparent distinction between powerful SSCSs which are identified with QSOs and those identified with galaxies. Recent MERLIN and EVN maps show that the QSOs more often contain radio sources with peculiar structures while the structures of the galaxies are usually more linear[26]. We feel that this evidence points towards a relationship between the QSO phenomenon and the distortions visible in many powerful SSCSs—of which 3C380 is currently the best studied example. It is plausible that interstellar gas, highly energized as a result of a galaxy merger, forms part of the link.

Finally, Fig. 1 suggests to us that rotation has had a major role in the recent history of 3C380. If we then speculate that both the curious curving features associated with the nucleus and the compact knots (Fig. 2) are coeval and were produced in the same way, then the centre of rotation cannot be at the nucleus but must be offset to the south-east by $\sim$1.5 arc s. This is consistent with the galaxy merger hypothesis if one of the galaxies is radio quiet while the other contains the radio source. The two galaxies will orbit their mutual centre of mass and so the centre of rotation will not be at the radio nucleus.

These first really detailed maps of a powerful SSCSs, the quasar 3C380, reveal an unexpected structure for a source of this luminosity but we cannot explain why the radio emitting plasma is distributed in this odd way. A circumstantial case can be made that the energy-carrying beams are interacting with energetic interstellar gas resulting from a galaxy merger, but the merger hypothesis cannot be proven until we have a better optical image of the QSO, perhaps from the Space Telescope. Nevertheless, in the more immediate future radio polarization maps should give us a good idea of whether or not there is sufficient ionized gas around the radio components for the gas interaction hypothesis to be tenable.

We thank many colleagues for the efficient operation of MERLIN and the EVN, Bev and Derek Wills and Richard Simon for permission to quote unpublished results, Ger de Bruyn for the Westerbork data reduction and Robin Conway, Ian Browne and Colin Lonsdale for helpful discussions. P.N.W. acknowledges receipt of an SERC Advanced Fellowship.

Received 16 January; accepted 10 February 1984.

1. Rees, M. J. *IAU Symp.* No. 97, 211–222 (1982).
2. Blandford, R. D. & Konigl, A. *Astrophys. J.* **232,** 34–48 (1979).
3. Orr, M. & Browne, I. W. A. *Mon. Not. R. astr. Soc.* **200,** 1067–1080 (1982).
4. Kapahi, V. K. *Astr. Astrophys. Suppl.* **43,** 381–393 (1981).
5. Peacock, J. & Wall, J. V. *Mon. Not. R. astr. Soc.* **198,** 843–860 (1982).
6. Davies, J. G., Anderson, B. & Morison, I. *Nature* **288,** 64–66 (1980).
7. Cornwell, T. J. & Wilkinson, P. N. *Mon. Not. R. astr. Soc.* **196,** 1067–1986 (1981).
8. Readhead, A. C. S. & Wilkonson, P. N. *Astrophys. J.* **235,** 11–17 (1980).
9. Pearson, T. J. & Readhead, A. C. S. *Astrophys. J.* **248,** 61–81 (1981).
10. Hartas, J. S., Rees, W. G., Scott, P. F. & Duffett-Smith, P. J. *Mon. Not. R. astr. Soc.* **205,** 625–636 (1983).
11. Fanaroff, B. L. & Riley, J. M. *Mon. Not. R. astr. Soc.* **167,** 31P–35P (1974).
12. Miley, G. K. *A. Rev. Astr. Astrophys.* **18,** 165–218 (1980).
13. van Albada, G. D. & van der Hulst, J. M. *Astr. Astrophys.* **115,** 263–269 (1982).
14. Condon, J. J., Condon, M. A., Gisler, G. & Puschell, J. J. *Astrophys. J.* **252,** 102–124 (1982).
15. Blandford, R. D. & Konigl, A. *Astrophys. Lett.* **20,** 15–21 (1979).
16. Hargrave, P. J. & Ryle, M. *Mon. Not. R. astr. Soc.* **166,** 305–307 (1974).
17. Gower, A., Gregory, P. C., Hutchings, J. B. & Unruh, W. G. *Astrophys. J.* **262,** 478–496 (1982).
18. Wilson, A. S. & Ulvestad, J. S. *Astrophys. J.* **236,** 576–594 (1982).
19. Heckman, T. M., Miley, G. K., Balick, B., van Breugel, W. J. M. & Butcher, H. R. *Astrophys. J.* **262,** 529–553 (1983).
20. van Breugel, W. J. M., Heckman, T. M., Butcher, H. R. & Miley, G. K. *Astrophys J.* **277,** 82–91 (1984).
21. van Breugel, W. J. M., Miley, G. K. & Heckman, T. M. *Astr. J.* **89,** 5–22 (1984).
22. Stockton, A. & MacKenty, J. W. *Nature* **305,** 678–682 (1983).
23. Hutchings, J. B. & Campbell, B. *Nature* **303,** 584–588 (1983).
24. Bothun, G. D. *et al. Astr. J.* **87,** 1621–1627 (1982).
25. Balick, B. & Heckman, T. M. *Astrophys. J.* **265,** L1–L5 (1983).
26. Wilkinson, P. N., Spencer, R. E., Readhead, A. C. S. & Simon, R. S. *IAU Symp.* No. 110 (in the press).
27. Boroson, T. A. & Oke, J. B. *Nature* **296,** 397–399 (1982).

A new model for the role of the oceans in determining atmospheric P_{CO_2}

J. L. Sarmiento & J. R. Toggweiler

Geophysical Fluid Dynamics Program, Princeton University, Princeton, New Jersey 08542, USA

Recent ice-core measurements have revealed that the atmospheric CO_2 level increased comparatively rapidly by about 70 p.p.m. at the end of the last ice age[1]. Here we present an ocean–atmosphere model in which changes in the productivity of high latitude surface waters (from which deep water is formed and circulated around the world's ocean) and/or in the thermohaline overturning rate can lead to substantial changes in atmospheric partial pressure of carbon dioxide (P_{CO_2}), over a concentration range 163–425 p.p.m. A major contribution to the low P_{CO_2} of the last ice age may have been an increase in the net high latitude productivity, possibly coupled with a decrease in the thermohaline overturning.

Figure 1 shows that three-quarters of the ocean volume, approximately everything below 1 km depth, interacts with the atmosphere through $\leq$4% of the ocean's high latitude surface area. The time scale of this interaction is of the order of 1,000 yr (ref. 2). An additional 16% of the ocean volume interacts with the atmosphere through 16% of the surface area on a time scale of the order of 10–100 yr (ref. 3). The processes occurring in these very small areas of contact between the deep ocean and the atmosphere are very important because of the large volume of ocean involved.

GEOSECS and TTO data show that freshly formed deep waters, those most recently in contact with the atmosphere, have P_{CO_2} and P_{O_2} approximately equal to atmospheric levels, and nutrient concentration levels between those of deep water and depleted low latitude surface water. Most simple models of the ocean–atmosphere system, in which the contact between the deep ocean and atmosphere is represented either through a surface box of nutrient-depleted low latitude water[4–6] or by direct contact[6,7] are inconsistent with these observations. In the latter case, the nutrient concentrations at the deep water outcrop will be those of deep water, far higher than observed. More significantly, the P_{O_2} and P_{CO_2} will be those of deep water, much too low for O_2 and too high for CO_2.

Figure 2 shows our 4-box model of the ocean–atmosphere. It differs from most other ocean box models in that the deep water contacts the atmosphere predominantly through a high latitude box that has properties somewhere between those of nutrient-depleted low latitude surface waters and nutrient-enriched deep waters. The addition of a high latitude box in our model makes it possible to form deep water with appropriate characteristics.

We will discuss the solution of the equations for the 4-box model elsewhere (J.R.T. and J.L.S., in preparation). An excellent approximation can be obtained by leaving out the intra-ocean fluxes from low latitude surface water, f_{ld} and f_{lh}. The reduction in the number of variables allows us to use the carbon-14 distribution in combination with the PO_4, AOU (apparent oxygen utilization, used instead of O_2), ΣCO_2, and alkalinity (ALK), to place strong constraints on the magnitude of the overturning, T and f_{hd} (see Fig. 2 legend for conventions).

We first discuss a solution of our box model for the modern ocean. The particle fluxes p_l and p_h (l refers to low latitude and h to high latitude) into the deep ocean are obtained in terms of PO_4 so that PO_4 is our master variable, although one could as easily use NO_3. Zero PO_4 concentration is assumed in the low latitude surface box:

$$p_l = TPO_{4d} \quad (1)$$

$$p_h = PO_{4d} f_{hd} - PO_{4h}(f_{hd} + T) \quad (2)$$

The conservation equations for AOU, ΣCO_2 and ALK in the deep box then give:

$$PO_{4h} = PO_{4d} - (AOU_d)/r_{O_2/PO_4} \quad (3)$$

$$\Sigma CO_{2h} = \Sigma CO_{2d} - r_{C/PO_4}(PO_{4d} - PO_{4h}) \quad (4)$$

$$ALK_h = ALK_d - r_{ALK/PO_4}(PO_{4d} - PO_{4h}) \quad (5)$$

r_{O_2/PO_4} is the Redfield ratio of O_2 needed to completely oxidize organic matter. We use $r_{O_2/PO_4} = 136$ (refs 5, 8) and r_{C/PO_4}, which includes the carbon in $CaCO_3$, is 131 (refs 5, 8). r_{ALK/PO_4} is 38 (refs 5, 8).

We have assumed that $AOU_h = 0$, that is, oxygen is in atmospheric equilibrium. We use equation (3) to find PO_{4h} from measurements of PO_{4d} and AOU_d. If $AOU_h > 0$, as may be the case where deep water is forming very rapidly, PO_{4h} would be slightly larger and our results would have to be modified accordingly. Equations (4) and (5) are used to obtain estimates of ΣCO_{2h} and ALK_h from measured estimates of ΣCO_{2d} and ALK_d.

The balance of alkalinity and carbon in the low latitude surface box, and of carbon dioxide in the atmosphere gives us:

$$ALK_l = ALK_d - r_{ALK/PO_4}(PO_{4d}) \quad (6)$$

$$\Sigma CO_{2l} = \Sigma CO_{2d} - r_{C/PO_4}(PO_{4d}) + f_{al}\,\beta(\theta_l)(P_{CO_{2a}} - P_{CO_{2l}})/T \quad (7)$$

$$\beta(\theta_h) f_{ah}(P_{CO_{2a}} - P_{CO_{2h}}) = \beta(\theta_l) f_{al}(P_{CO_{2a}} - P_{CO_{2l}}) \quad (8)$$

Table 1 Model predictions

		Present pre-industrial	Ice age scenario
Model parameters	p_h (mol Cs^{-1})	2.31×10^{6}*	11.48×10^{6}
	f_{hd} (m^3s^{-1})	38.1×10^{6}	38.1×10^{6}
	T (m^3s^{-1})	25.4×10^{6}	9.0×10^{6}
Atmosphere	P_{CO_2} (p.p.m.)	265	200
High latitude surface ocean	PO_4 ($\mu M\,kg^{-1}$)	1.02	0
	ΣCO_2 ($\mu M\,kg^{-1}$)	2,121	2,213
	ALK (μequiv. kg^{-1})	2,329	2,517
	P_{CO_2} (p.p.m.)	259	185
Low latitude surface ocean	ΣCO_2 ($\mu M\,kg^{-1}$)	1,941	2,044
	ALK (μequiv. kg^{-1})	2,290	2,517
	P_{CO_2} (p.p.m.)	269	205
Deep ocean	PO_4 ($\mu M\,kg^{-1}$)	2.15	2.24
	AOU† ($\mu M\,kg^{-1}$)	154	305
	ΣCO_2 ($\mu M\,kg^{-1}$)	2,269	2,506
	ALK (μequiv. kg^{-1})	2,372	2,601

* This flux is equivalent to 1.39 mol C m^{-2} yr^{-1}.
† Deep ocean $O_2 + AOU \sim 320$ $\mu M\,kg^{-1}$.

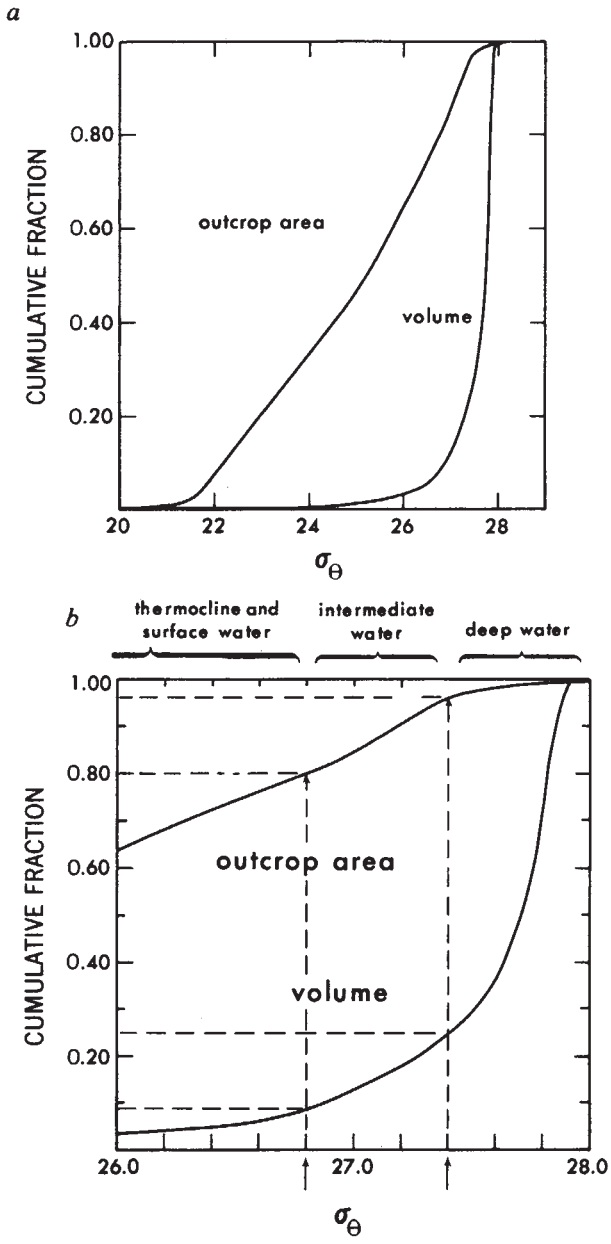

Fig. 1 NODC hydrographic data mapped by Levitus[14] for the three winter months have been used to calculate surface outcrop areas and interior volumes contained in σ_θ intervals of 0.1. σ_θ is potential density referred to the surface. The figure shows the cumulative fraction of these two quantities. For example, 75% of the ocean volume has a $\sigma_\theta > 27.4$. Water in this density range outcrops in <4% of the surface ocean.

The β values are solubilities of CO_2 in waters of temperature $\theta_l = 21.5$ °C, and $\theta_h = 2.5$ °C respectively. The solubilities are obtained from the equations of Takahashi *et al.*[9], as are $P_{CO_{2l}}$ and $P_{CO_{2h}}$. The latter are functions of the temperature, salinity (we use 34.7‰ for the present ocean), alkalinity and total carbon. We have used Broecker and Peng's[4] estimates of gas exchange rates from radon-222 measurements to obtain $f_{ah} = 3$ m day$^{-1} \times 0.15 \times$ (ocean area) and $f_{al} = 3$ m day$^{-1} \times 0.85 \times$ (ocean area).

We now have eight equations, 10 if we include the Takahashi equations for $P_{CO_{2l}}$ and $P_{CO_{2h}}$, with 15 'unknowns'. We use GEOSECS and TTO data to find PO_{4d}, AOU_d and ALK_d. ΣCO_{2d} can also be estimated from data, but it includes a fossil fuel component, so we prefer to specify $P_{CO_{2a}} = 265$ p.p.m. (ref. 1) and calculate ΣCO_2 from the data. T and f_{hd}, which do not enter into equations (1) to (8), are obtained by consideration of radiocarbon observations (J.R.T. and J.L.S., in preparation).

The first column of Table 1 gives our best estimates of the present pre-industrial model variables. Our predicted value for the deep ocean ΣCO_2, 2,269 μm kg^{-1}, compares very well with our estimate of 2,274 μm kg^{-1} from GEOSECS and TTO data.

We now turn to a consideration of how the ocean and atmosphere change in response to changes in the physical processes, f_{hd} and T, and the high latitude productivity, p_h. We find that the results are very sensitive to whether or not one conserves total tracer in the ocean–atmosphere system. We thus add three new equations to our model: conservation of total alkalinity, carbon and phosphate. This also adds three new 'unknowns', ALK_t, ΣCO_{2t} and PO_{4t}, where t refers to total. We now have 13 equations and 19 'unknowns', including now f_{hd} in the unknowns. We solve the equations by specifying the total alkalinity, carbon and phosphate, as calculated from present values in Table 1. f_{hd}, T and P_h are also specified as some fraction of the present ocean values.

Because of the way we have set up our equations, using phosphate as a master variable, the parameters f_{hd}, T and p_h enter into only three of them: equations (1), (2) and (7). If we substitute equation (2) into the total phosphate conservation equation, we arrive at:

$$PO_{4h} = (M_t PO_{4t} - M_d p_h / f_{hd}) / [M_h + M_d(1 + T/f_{hd})] \quad (9)$$

where M is the mass of a given reservoir in kg.

Consideration of this equation in combination with equation (7) reveals the role of f_{hd}, T and p_h. Consider, first, the high latitude particulate flux, p_h. If this is decreased to zero, the high latitude phosphate will reach a maximum value, with ΣCO_{2h} and ALK_h following suit. The $P_{CO_{2h}}$ will thus also be at its maximum value. Conversely, an increase of p_h, because of its effect on PO_{4h}, will lead to a decrease in PO_{4h}, ΣCO_{2h}, ALK_h and $P_{CO_{2h}}$, with an absolute minimum reached when PO_{4h} is zero.

However, the atmospheric P_{CO_2} depends on the low latitude P_{CO_2} as well as the high latitude P_{CO_2} (equation (8)), and we must thus consider equation (7) as well. The sensitivity of low latitude ΣCO_2 and P_{CO_2} to the high latitude processes depends on the magnitude of T. If T is very large, that is, if the low latitude surface waters are being resupplied very rapidly from deep waters, the low latitude waters will be relatively insensitive to high latitude processes. A small T will mean that the low latitude carbon concentration will be determined primarily by the atmosphere, which will in turn be dominated by high latitude waters.

The effect of variations in f_{hd} can be seen from equation (9); f_{hd} supplies nutrients to the high latitude waters. An increase in f_{hd} increases PO_{4h}, a decrease in f_{hd} decreases PO_{4h}.

The arguments given above are illustrated with the solutions in Fig. 3. In Fig. 3*a*, f_{hd} is fixed and p_h and T are varied about the values $p_h°$ and $T°$ taken from the present pre-industrial column of Table 1. For large T, the atmospheric P_{CO_2} approaches a value of 250 p.p.m. and is not sensitive to p_h. The sensitivity of atmospheric P_{CO_2} to p_h increases greatly as T is reduced.

In Fig. 3*b*, p_h is fixed and f_{hd} and T are varied about the values $f_{hd}°$ and $T°$. One sees that the effect of f_{hd} on P_{CO_2} is essentially the inverse of the effect of p_h on P_{CO_2}.

Figure 3*c* shows a possible range of scenarios for the last ice age. We have fixed f_{hd} and varied p_h, but one would obtain the same effect by varying f_{hd}. It can be seen from Fig. 3*c* that a decrease of atmospheric P_{CO_2} to 200 p.p.m. (ref. 9) requires a rather extreme increase in p_h (decrease of f_{hd}) of the order of 4–5 times, accompanied by about a halving of T. The total ocean volume of our ice age model has been decreased by 3.5% to account for glacier formation. The total carbon and alkalinity have been increased by 6% to account for the shift in $\delta^{13}C$ and a compensatory gain of $CaCO_3$ from the sediments as postulated by Broecker[5]. This increase in carbon and alkalinity makes it more difficult to achieve the lower P_{CO_2} found for the last ice age.

The work of Boyle and others gives evidence of a drop in North Atlantic deep water formation during the last ice age[10,11]. This would translate into a drop in f_{hd} and/or T in our model. A decrease in f_{hd} would be helpful. A decrease in T would be helpful, if accompanied by a sufficient increase in productivity or decrease in f_{hd}. A likely cause of changes in surface production is a change in the light supply to the subpolar gyres. Organism growth in these areas is presently light-limited. The gyres straddle the present polar night line (~60°N). A shift in the deep water formation regions to lower latitudes by sea ice blockage of higher latitudes would drive the water to regions where organisms would have a more ample light supply. We consider it unlikely that p_h would increase sufficiently to explain the entire decrease in P_{CO_2}. A decrease in f_{hd} would help.

A critical test of the various models for predicting ice age P_{CO_2} is the extent to which they can give the observed rapid time scales of the change. Our model allows us to develop a scenario involving only a change in p_h and T, which would adjust on a time scale of the order of 1,000 yr. This is consistent with the data[1]. The scenario in Fig. 3*c* as well as Broecker's[5], would take about 5,000 yr because of the need to readjust the $CaCO_3$ balance in the oceans. Five thousand years is longer than the data allow. The increase in oceanic carbon required by the $\delta^{13}C$

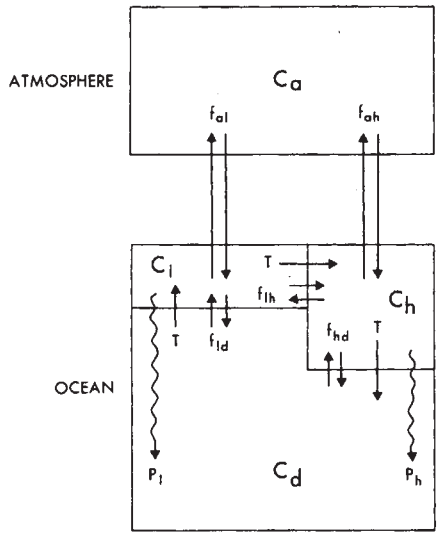

Fig. 2 Schematic diagram of our 4-box model. f, Exchange rates in units of m^3 s^{-1}. Subscripts: a, atmosphere; l, low latitude nutrient-depleted surface water; h, high latitude deep water formation regions; d, deep ocean. In addition to exchange rates, the model allows for a shallow thermohaline overturning, T(m^3 s^{-1}), which goes through the low latitude surface box to the high latitude surface box before sinking into the deep box. p (mol C s^{-1}), Total particulate flux of organic and carbonate carbon. We assume that none is lost to sediments. We visualize the low latitude surface box as being 100 m thick and occupying 85% of the ocean's surface area. The high latitude surface box, which represents essentially the subpolar gyres, is 250 m thick and occupies the remaining 15% of the surface ocean.

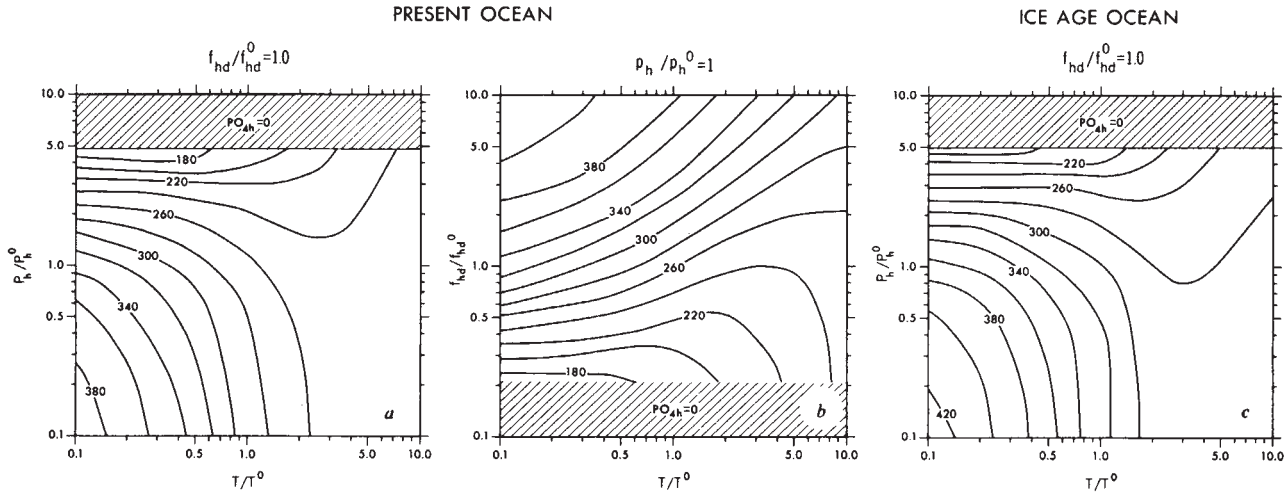

Fig. 3 Atmospheric P_{CO_2} (in p.p.m.) as predicted by our model for various values of the parameters f_{hd}, p_h and T. $f_{hd}^0 = 38.1 \times 10^6\ m^3\ s^{-1}$, $p_h^0 = 2.31 \times 10^6$ mol C s^{-1}, and $T^0 = 24.5 \times 10^6\ m^3\ s^{-1}$. (See text for a description of the various scenarios.) The ice age ocean has an ocean volume that has been decreased by 3.5% and a total carbon and alkalinity content increased by 6%.

signal, and the precipitation of $CaCO_3$ which would have to accompany it, poses a dilemma. A time-dependent model is needed to study the problem in more detail.

Changes in the tilt of the Earth's axis, which would affect particularly the high latitude winter insolation, may actually drive the climate through the CO_2 response we have discussed here. The extremes within which the P_{CO_2} could conceivably vary with the present ocean volume, total carbon and alkalinity, and value of T, are ~190 p.p.m. to 300 p.p.m. If T were to approach zero the P_{CO_2} could vary between ~163 and 425 p.p.m. The climatic effect of P_{CO_2} changes within this range would be considerable. Manabe and Stouffer[12] as well as many others have shown that a halving or doubling of P_{CO_2} should lead to a decrease or increase of ~2 °C in global mean temperature.

Changes in the oceanic carbon distribution by the processes represented by T, f_{hd} and P_h, may also have an impact on fossil fuel uptake. It is difficult to tell what the effect would be. A decrease in T and/or f_{hd} might be expected as high latitude surface waters warm up. A decrease in T and f_{hd} would affect the CO_2 uptake in opposite directions (see Fig. 3). We have not studied this problem, but suspect the effect of variations in T, f_{hd} and p_h on CO_2 uptake would be relatively small because of a tendency for the effects of T and f_{hd} to cancel each other out and because of the short time scales of the fossil fuel CO_2 transient relative to large-scale oceanic overturning.

Evidence of the types of changes we have suggested here for the ice ages should be available in sediment records. An increase in high latitude productivity should lead locally to fairly dramatic increases in sedimentation rates. The palaeo-PO_4, which Boyle estimates by Cd measurements in foraminifera[10], should be lower near deep water formation regions. Table 1 shows that the deep ocean oxygen levels would have decreased enormously in the extreme conditions of the ice age. One would expect anoxia to have been widespread at the depth of the oxygen minimum with possible effects on the sediments and trace metal distributions. We are presently seeking confirmation of our hypothesis in data of this sort, as well as working on the development of a three-dimensional ocean circulation model of the carbon cycle that will more realistically simulate the effect of high latitude productivity and thermohaline overturning rate on atmospheric P_{CO_2}.

We acknowledge support from ARL/NOAA grant NA83RAC00052, NSF grant OCE-8110155, and GFDL/NOAA grant 04-7-022-44017. We also appreciate the help of Sol Hellerman and Marty Jackson in data analysis, Johann Callan in typing the manuscript, and Phil Tunison in drafting the figures. This paper is based on material first presented at a NATO Advanced Research Institute in July 1983. After this paper was accepted for publication we discovered that Oeschger *et al.*[13] were the first to suggest the idea we explore here.

Received 16 November 1983; accepted 1 January 1984.

1. Neftel, A. H., Oeschger, H., Schwander, J., Stauffer, B. & Zumbrunn, R. *Nature* **295,** 220–223 (1982).
2. Broecker, W. S. in *The Sea* Vol. 2 (ed. Hill, M. N.) 88–108 (Interscience, New York, 1963).
3. Sarmiento, J. L. *J. phys. Oceanogr.* **13,** 1269–1274 (1983).
4. Broecker, W. S. & Peng, T.-H. *Tracers in the Sea* (Eldigio, Palisades, 1982).
5. Broecker, W. S. *Geochim. cosmochim. Acta* **46,** 1689–1705 (1982).
6. Broecker, W. S. & Takahashi, T. *Ann. Glaciol.* (submitted).
7. Siegenthaler, U. *J. geophys. Res.* **88,** 3599–3608 (1983).
8. Redfield, A. C., Ketchum, B. H. & Richards, F. A. *The Sea* Vol. 2 (ed. Hill, M. N.) 26–75 (Interscience, New York, 1963).
9. Takahashi, T., Broecker, W. S., Bainbridge, A. E. & Weiss, R. F. *Tech. Rep.* No. 1, CU-1-80 (Lamont-Doherty Geol. Observatory, Palisades, New York, 1980).
10. Boyle, E. A. & Keigwin, L. D. *Science* **218,** 784–787 (1982).
11. Streeter, S. S., Belanger, P. E., Kellogg, T. B. & Duplessey, J. C. *Quat. Res.* **18,** 72–90 (1982).
12. Manabe, S. & Stouffer, R. J. *J. geophys. Res.* **85,** 5529–5554 (1980).
13. Oeschger, H. *et al. Maurie Ewing Symp. 1982* Vol. 4 (American Geophysical Union, Washington DC, in the press).
14. Levitus, S. *Climatological Atlas of the World Ocean* (NOAA Professional Pap. 13, US Dept. of Commerce, Washington DC, 1982).

Rapid atmospheric CO_2 variations and ocean circulation

U. Siegenthaler & Th. Wenk

Physics Institute, University of Bern, CH-3012 Bern, Sidlerstrasse 5, Switzerland

Studies on air trapped in old polar ice[1,2] have shown that during the last ice age, the atmospheric carbon dioxide concentration was probably significantly lower than during the Holocene—about 200 p.p.m. rather than 270 p.p.m. Also, Stauffer *et al.*[3] recently showed by detailed analyses of Greenland ice cores, that during the ice age, between about 30,000 and 40,000 yr BP, the atmospheric CO_2 level probably varied between 200 and 260 p.p.m. These variations occurred parallel to climatic variations as indicated by $\delta^{18}O$ of the ice; astonishingly, the changes took place within rather short times, no more than a few centuries or even less. Here we examine the hypothesis[4] that CO_2 variations arose from changes in ocean circulation that affected the distribution of chemical properties and thus of P_{CO_2} in the surface waters of the world ocean. Such changes can take place in a rather short time, in contrast to changes of whole ocean properties.